RSC Advances

PAPER

View Article Online
View Journal | View Issue

Cite this: *RSC Adv.*, 2018, **8**, 3839

Enhanced moisture sensing properties of a nanostructured ZnO coated capacitive sensor

Harinder Singh,[a] Akshay Kumar,[a] Babankumar S. Bansod,[b] Tejbir Singh,[c] Anup Thakur,[d] Tarandip Singh[e] and Jeewan Sharma *[a]

Received 3rd October 2017
Accepted 23rd December 2017

DOI: 10.1039/c7ra10917b

rsc.li/rsc-advances

This work reports the enhancement in sensitivity of a simple and low-cost capacitive moisture sensor using a thin film of zinc oxide (ZnO) nanoparticles on electrodes. The ZnO nanoparticles are systematically characterized using X-ray diffraction, atomic force microscopy, transmission electron microscopy, BET surface area analysis, Fourier transform infrared spectroscopy, and UV-visible and photoluminescence (PL) spectroscopy. The average crystallite size of the ZnO nanoparticles is ~16 nm with a surface roughness of ~3 nm. Blue emission in the PL spectrum confirms the presence of oxygen vacancy dipoles, which are responsible for enhancing the dielectric properties of the ZnO nanoparticles. The effect of the ZnO nanoparticles on the sensitivity of a moisture sensor cell has been studied using wheat grains with a moisture content from 7% to 25%. An enhancement in sensitivity of 36.4% at 1 MHz and 97.4% at 500 Hz has been observed. A detailed sensing mechanism is proposed and the enhancement in sensing has been explained based on the interaction of ZnO with water vapor and the dielectric behavior of the nanostructured ZnO. The present results establish ZnO as a sensing material for improving the utility of moisture sensors.

1 Introduction

The measurement of moisture/humidity has great importance in various industry related and commercial applications, such as the monitoring of environment, industrial processes, soil, medicine analysis industries, food grains and beverages.[1] Food is one of the important requirements for the survival of living organisms, so its safe storage is a highly important issue for a nation's economy. Post-harvest losses badly affect the sustainability of the food ecosystem. During harvest, high moisture levels in food grains can deteriorate or ferment them. Therefore, it is important to measure precisely the grain moisture levels. The basic principle of a humidity/moisture sensor is based on the change in the refractive index (optical),[2] mass (gravimetric),[3] dielectric constant (capacitive)[4,5] or in the conductivity (resistive)[6–8] of the active material with the moisture content. Furthermore, the essential properties of moisture sensors for their extensive use include low cost, high sensitivity, precision and good performance.[9] Amongst various moisture sensors, the capacitance measurement based sensor became most popular due to numerous merits such as being non-destructive, fast response time, small sampling volumes, higher accuracy and low cost.[10,11] In the case of food grains, the capacitance value depends upon many factors[9] and can be expressed using eqn (1)

$$C_c = K_0 e\varepsilon_a + K_0(1-e)\varepsilon_g + \frac{K_0\gamma_g(1-e)(\varepsilon_w-\varepsilon_g)}{1+M(\gamma_g-1)}M \quad (1)$$

where $K_0 = (\varepsilon_0 A)/D$ with A as the area and D as the distance between the two electrodes, ε_0 is the dielectric constant of vacuum, M is the grain moisture, ε_g is the dielectric constant of grains, ε_w is the dielectric constant of water, ε_a is the dielectric constant of the air between grains, γ_g is the volume of grains and e is the rate of air gaps. From the equation it is clear that, along with others, moisture is an important factor in determining the capacitance. The type of grain also affects the measurements as different grains have different dielectric constants. The rate of grain gaps is the main factor that affects precision and should be eliminated. However, the capacitive signal in a moisture sensor cell depends upon different geometrical constraints such as the surface area of the electrode and the space between the electrodes,[12] which become constant once the sensor fabrication has been completed. These constraints limit the performance of existing sensors. Visualizing this, Qi *et al.*[13] proposed the efficient utilization of nanoparticles for improving the moisture and humidity sensing properties because of their high density of surface states and

[a]*Department of Nanotechnology, Sri Guru Granth Sahib World University, Fatehgarh Sahib, 140 407, India. E-mail: jeewansharma29@gmail.com*
[b]*Central Scientific Instruments Organization, Chandigarh, 160 030, India*
[c]*Department of Physics, Sri Guru Granth Sahib World University, Fatehgarh Sahib, 140 407, India*
[d]*Department of Basic and Applied Sciences, Punjabi University, Patiala, Punjab, 147 002, India*
[e]*Department of Electronics Engineering, Sri Guru Granth Sahib World University, Fatehgarh Sahib, 140 407, India*

quantization effects. In capacitive sensors, the modification of capacitor electrodes with nanomaterials is one of the strategies used to enhance their performance as it leads to an increase in the accumulation of water vapor on the surface and diffusion into it.

ZnO is a group II–VI, wide band gap (3.3 eV) semiconducting compound[14] with a stable wurtzite structure[15] and can be synthesized in various morphologies.[16–19] It exhibits distinctive properties and is widely applicable as an electrical generator,[20] or in light emitting diodes,[21] solar cells,[22] and different types of gas, as well as humidity, sensor.[18,23,24] Due to the high chemical stability, low cost, non-toxic nature, chemical sensitivity to gases, ease of doping and enhanced dielectric properties, ZnO nanoparticles were conceived to be beneficial in gas sensing applications and moisture detection.[25] ZnO nanoparticles have been synthesized using different alkaline solutions.[26–28] Im *et al.*[26] suggested that in alkaline solutions, ZnO nanoparticles are more stable and have few aggregates. Furthermore, they reported that ZnO nanoparticles obtained using LiOH show excellent electrochemical performance, high discharge capacity and small charge transfer resistance (R_{ct}). Moreover, the maximum yield of ZnO nanoparticles has been obtained using LiOH among different alkaline hydroxides.[27] Recently, it has been reported that LiOH can act as a very efficient base to control the synthesis and hence the properties of ZnO nanoparticles.[28]

In the present report, ZnO nanoparticles are synthesized using LiOH as a precursor and characterized using different techniques. Furthermore, efforts are made to visualize the enhancement in the sensitivity of a capacitive moisture sensor by depositing nanostructured ZnO thin films on cell electrodes. The modified and low cost sensor has been used to measure the capacitive signal for different moisture concentrations (7–25%) in wheat.

2 Materials and methods

The established experimental set up included a capacitive sensor cell as the sensing system followed by an LCR meter for data measurement and acquisition. The rectangular cell was fabricated from an acrylic sheet with outer dimensions of 44.0 mm × 41.5 mm × 11.5 mm, as shown in Fig. 1. Stainless steel sheets with dimensions of 42.7 mm × 33.4 mm were used for the electrodes. The space (d) between the electrodes was 10.5 mm. These electrodes were coated with a nanocrystalline ZnO thin film using a 1000S Milman spin coating unit.[29]

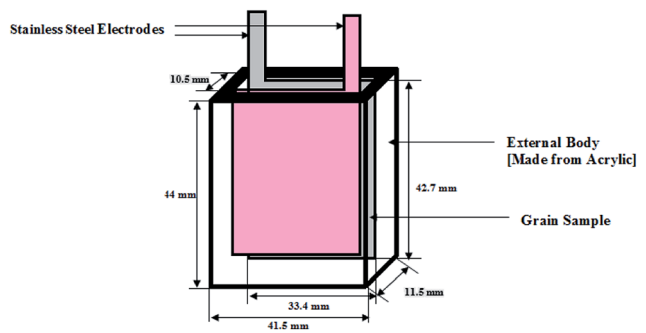

Fig. 1 Structural view of the moisture sensor cell.

A wet chemical method was used to synthesize the ZnO nanoparticles with zinc acetate and lithium hydroxide as the precursors. The chemicals of AR grade were procured from Sigma Aldrich, India. The solutions of zinc acetate and lithium hydroxide were prepared by dissolving 3.35 mmol of $Zn(Ac)_2 \cdot 2H_2O$ in 31.25 ml of methanol and 6.59 mmol of lithium hydroxide powder in 50 ml of methanol under continuous stirring, respectively. Lithium hydroxide solution was added dropwise to zinc acetate solution with continuing stirring at 60 °C. After one and a half hours, the solution became turbid and ZnO nanoparticles started to precipitate. The solution was kept undisturbed for another 2 hours. The zinc oxide nanocrystals were filtered and washed twice with methanol.

The wheat grain samples with a specified moisture content were prepared as specified in ISO 712:2009.[30] Four wheat samples with a 7%, 15%, 20% and 25% moisture content were prepared. For each sample, 50 g of wheat was stored in dried, cleaned and airtight polythene bags. The required quantity of deionized water was introduced into the bags and the samples were shaken energetically for 4 days. All of the wheat samples were stored at 2–6 °C and sealed after ensuring uniform distribution of water (moisture).[31] The samples so prepared were then introduced into the sensor cell and the capacitance was measured using a data logging system. An LCR meter (QuadTech 1920) was used to record the capacitance of the sensor cell. These observations were recorded in the frequency range from 500 Hz to 1 MHz. Before starting the measurements, the sensor was calibrated properly for the wheat samples with differing moisture content.[32] The variations in the grain size and rate of grain gaps were taken care of by repeating the experiment three times and the average value of the capacitance was considered. The stability of the sensor was ensured by repeating the experiment twice with an interval of one month. The distance between the electrodes was fixed and all of these measurements were recorded at room temperature. X-ray diffraction (XRD) spectrum was recorded using an XPERT-PRO X-ray diffractometer, with $CuK_\alpha 1$ radiation with $\lambda = 1.54060$ Å. To study the morphological features, transmission electron microscopy (TEM) images were obtained on an FEI: FP 5022/22-Tecnai G2 20 S-Twin microscope. The specific surface area of the sample was measured with the Brunner–Emmet–Teller (BET) method using a nitrogen adsorption system (Microtrac Belsorp Mini-II). The Fourier transform infrared spectroscopy (FTIR) spectrum was recorded using a BRUKER-ALPHA spectrometer in the spectral range of 4000 to 300 cm^{-1}. A UV-visible spectrum was obtained using a U-3900H UV-visible spectrophotometer. A fluorescence spectrophotometer (VARIAN) was used to study the photoluminescence (PL) behavior of ZnO. atomic force microscopy (AFM) images were obtained using a Veeco Explorer Instrument (USA) in contact mode over a scanning area of 3 μm × 3 μm.

3 Results and discussion

Fig. 2(a) shows the XRD spectrum of the synthesized material along with the standard pattern. The XRD analysis confirms the synthesis of hexagonal ZnO [JCPDS data file no. 00-003-

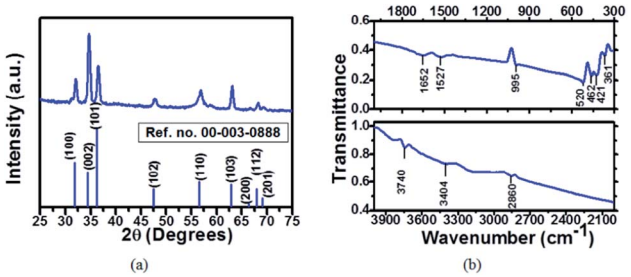

Fig. 2 (a) The XRD pattern of the ZnO nanoparticles along with the standard data and (b) the FTIR spectrum of the ZnO nanoparticles.

0888]. The spectrum indicates the presence of peaks arising from (100), (002), (101), (102), (110), (103) and (112) reflections from the polycrystalline ZnO [JCPDS data file no. 00-003-0888]. The average crystallite size (D) has been calculated using Scherer's equation

$$D = \frac{0.9\lambda}{\beta \operatorname{Cos} \theta} \quad (2)$$

where β is the full width at half maximum (FWHM), θ is the Bragg angle and λ is the wavelength of the incident X-ray beam. The average crystallite size of ZnO was calculated to be ~16 nm.

The FTIR spectrum of the ZnO nanoparticles in the spectral range of 4000 to 300 cm^{-1} is shown in Fig. 2(b). The band located at 460–520 cm^{-1} has been correlated to the stretching of Zn–O due to the E_2 mode of the hexagonal ZnO structure.[33] The peak at 3404 cm^{-1} confirms the presence of hydroxyl groups (O–H mode of vibration). The symmetrical bending mode vibration of C=O has been observed at 1527 cm^{-1}. A band at 2860 cm^{-1} was observed due to the symmetric C–H stretching vibrational mode.[34] There is an absorption band at 995 cm^{-1} corresponding to stretching of C–O bonds. This band confirms the presence of zinc acetate even after repeated washing of the samples.

Fig. 3(a and b) shows AFM images that confirm the good distribution of the ZnO nanoparticles along the surface. The

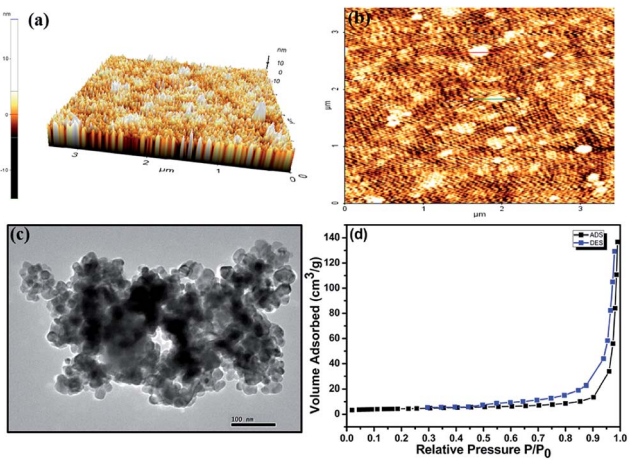

Fig. 3 (a, b) AFM images, (c) a TEM image and (d) the nitrogen adsorption–desorption isotherm of the ZnO nanoparticles.

Root Mean Square (RMS) roughness is considered as one of the most important parameters for characterizing the surface profile of a material. Analytically, it can be estimated using AFM as

$$R_q = \sqrt{\frac{1}{L}\int_0^L |Z^2(x)| dx} \quad (3)$$

where $Z(x)$ represents the surface profile that is analyzed in terms of position x and height Z of the sample evaluated over the length L. In the present case, the RMS roughness value has been estimated to be 3.13 nm using eqn (3). The rough surface supports the improvement in the sensitivity of the moisture sensor as it provides more moisture trapping sites and contributes to an increase in the effective surface area of the sensor electrodes. To understand the adhesion mechanism on the nanometer scale, the effect of the RMS roughness on the adhesion was studied using AFM.[35] It was suggested that roughness has a significant role in applications of microelectromechanical systems. Fig. 3(c) shows the TEM image of a ZnO powder sample, showing an average crystallite size in the range of ~15–20 nm. This value is in good agreement with the crystallite size calculated from the XRD results. Fig. 3(d) shows the nitrogen adsorption–desorption isotherm for the ZnO nanoparticles. This isotherm can be recognized as Type-IV, according to the IUPAC classification. Similarly, the hysteresis loop is of Type H3, suggesting the material to be mesoporous. The BET surface area of the ZnO nanoparticles is estimated to be 55.3 m^2 g^{-1} indicating high porosity.

Fig. 4(a) shows the absorption spectrum of the ZnO nanoparticles in the UV-visible region. The inset in the figure represents the variation of $(\alpha h\nu)^2$ with energy. A direct band gap value of 3.40 eV has been measured by extrapolating the straight line portion of this graph to the energy axis. A blue shift of 0.10 eV has been observed with respect to its bulk counterpart.[36] Borah *et al.*[37] obtained a blue shift of 0.58 eV due to the quantum confinement effect in ZnS nanoparticles with a size of 5.86 nm. A blue shift in the band gap of ZnO nanoparticles has also been observed with variation in the particle size from 14.69 nm to 5.57 nm.[38] It has been proposed that the shift in the absorption edge is due to the polycrystalline nature of ZnO. In polycrystalline materials, there is an increase of extended localization in the conduction and valence bands leading to blue shift in the absorption edge.[39] In the present study, the

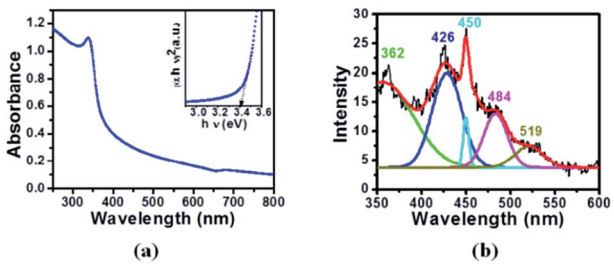

Fig. 4 (a) Absorption spectrum and an inset showing the variation of $(\alpha h\nu)^2$ with energy and (b) photoluminescence spectrum with a fitting profile for the ZnO nanoparticles excited at 330 nm.

main reasons for the blue shift are the surface roughness and the polycrystalline nature of the ZnO nanoparticles as quantum confinement dominates at much lower particle sizes in ZnO.

PL study of a material provides valuable information about the defect states and charge dynamics of the recombination mechanism.[40] Fig. 4(b) shows the PL curve of the ZnO nanoparticles over a wavelength range of 350 to 600 nm (excited at 330 nm). The emission spectrum was analyzed by fitting with multiple Gaussian curves. The fitting profile of the experimental data has a best fit with five peaks. The near-band-edge emission at 362 nm (UV region) is attributed to a free exciton–exciton recombination mechanism.[41] The appearance of a band in the visible region is due to the existence of deep level defects arising from zinc interstitials, oxygen vacancies and the attachment of hydroxyl groups in the lattice.[42] More specifically, the peak position at 426 nm corresponds to violet emission due to the transition from the conduction band to the deep hole trapped levels such as zinc vacancies (V_{Zn}).[43,44] Blue emissions at 450 nm and 484 nm can be associated with the transition due to the oxygen vacancy defects (O_{Zn}).[43,45] These oxygen vacancy defects act as dipoles and enhance the dielectric properties of the material.[46] The emission of green coloured light around 519 nm has been assigned to the presence of Zn and oxygen at interstitial positions.[47–49]

To check the effect of depositing ZnO nanoparticles on electrodes, the capacitance without and with ZnO deposition has been computed. Fig. 5 shows an improved equivalent electric circuit model suggested by Nahar *et al.*[50] for porous structured capacitor electrodes. Based on this equivalent circuit, the capacitance can be obtained as[50]

$$C = C_s + \frac{C_a C_b}{C_a + C_b} + C_{eff} \quad (4)$$

where C_s represents the capacitance of the capacitor walls, C_a represents the capacitance of the pore area filled with air, C_b is the capacitance of the barrier layer below the air portion, and C_{eff} denotes the capacitance of the multiple-dielectric capacitor comprising the sublayers: the barrier layer, the chemisorbed layer, and water condensed in the pore. On considering the actual porous structure of the ZnO nanoparticles, one can write the capacitance at any humidity level as[50]

$$C = \frac{\varepsilon_0 \varepsilon_s (1-\alpha) A}{d} + \varepsilon_0 \alpha A \left(\frac{x\varepsilon'}{d} + \frac{(1-x)\varepsilon_a \varepsilon_b}{\varepsilon_a b + \varepsilon_s l} \right) \quad (5)$$

where ε_0 is the permittivity of free space, ε_s the dielectric constant of ZnO (value), ε_a the dielectric constant of air (value 1), A the area of the device, α the film porosity, d the ZnO film thickness, b the barrier layer thickness, and l the length of the pore in which water can condense. The latter is the characteristic length of the sensor. x is the fraction of the pore area αA filled with water. ε' is the dielectric constant of the barrier layer chemisorbed layer-water structure.

Fig. 6(a) shows the variation of the capacitance with frequency for differing moisture content. There is an enhancement in the capacitive signal with deposition of the ZnO nanoparticles on the electrodes. To estimate the enhancement in the sensitivity, a parameter S, which is the ratio of change in the capacitance with unit change in moisture content, has been calculated using[51]

$$S = \frac{C_{25} - C_{15}}{M_{25} - M_{15}} \quad (6)$$

where C_{25} and C_{15} are the values of the capacitance at 25% (M_{25}) and 15% (M_{15}) moisture content, respectively. The value of the sensitivity (in pF/MC%) at different frequencies, with and without ZnO nanoparticles, has been calculated using eqn (6). Table 1 lists the values of the capacitance for the 15% and 25% moisture content samples along with the sensitivity (without and with ZnO) and the percentage enhancement in the sensitivity. The values of the sensitivity demonstrate the improved sensitivity of the moisture sensor due to deposition of the ZnO nanoparticles. Clearly, the sensitivity is frequency dependent and better sensitivity is obtained for lower frequencies. Capacitance *vs.* frequency data also support this behavior.

The variation of the capacitance with moisture content at frequencies of 500 Hz, 50 kHz, 500 kHz and 1 MHz is shown in Fig. 6(b). The enhancement in the capacitance is more prominent for lower frequencies even for the low moisture content samples. At higher frequencies, the capacitance decreases sharply due to the lack of polarization of the oxygen vacancy dipoles and adsorbed water molecules because these dipoles are not able to keep up with the rapid change in the electric field's direction due to inertia.[52] Thakur *et al.*[53] also reported a similar frequency dependence for a CeO_2 based humidity sensor. In the present work, the enhancement in the sensitivity is 97.4% at low frequency (500 Hz) and 36.4% at higher frequency (1 MHz). Lazarus *et al.*[54] obtained a sensitivity of

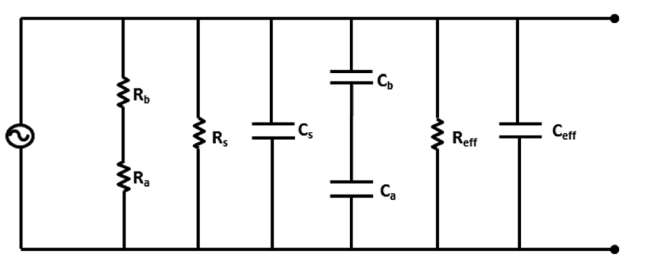

Fig. 5 Schematic of the electrical equivalent circuit model of a moisture sensor with ZnO nanoparticles on electrodes.

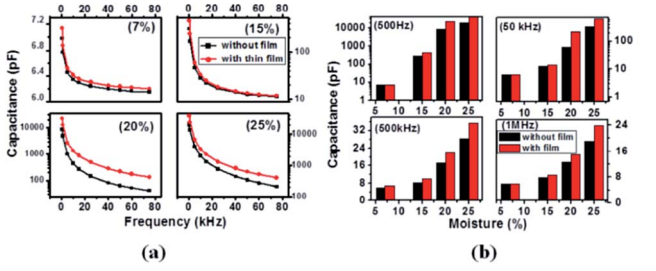

Fig. 6 Variation of the capacitance (a) with frequency at different moisture content and (b) with moisture content at different frequencies.

Table 1 Values of the capacitance, sensitivity (S) and percentage enhancement in the sensitivity (ES) at different frequencies (ω) for the moisture sensor cell with and without (W/O) ZnO nanoparticles

		Capacitance (pF)						
		Without ZnO		With ZnO		$S = \left(\frac{C_{25} - C_{15}}{M_{25} - M_{15}}\right)$ (pF/MC%)		
S. No.	ω (kHz)	15% MC	25% MC	15% MC	25% MC	Without ZnO	With ZnO	ES (%)
1	0.5	306.8	19 641.0	451.70	38 612.0	1933.4	3816.0	97.4
2	50.0	12.7	339.3	13.50	634.8	32.7	62.1	89.4
3	500.0	8.3	28.4	9.23	39.6	2.0	3.0	50.0
4	1000.0	7.8	19.0	8.64	23.8	1.1	1.5	36.4

0.31% pF/% RH for a parallel plate moisture sensor and Kumar[55] reported a similar type of humidity sensor (capacitive) using porous alumina with limited sensitivity at lower moisture content compared to our case.

Sensing mechanism

The enhancement in sensing, due to the ZnO nanoparticles, can be explained based on the interaction of ZnO with water vapor[56] along with the dielectric behavior of the nanostructured ZnO. The adsorption mechanism of water vapor on the ZnO nanoparticles is a combined effect of condensation of vapor within the capillary pores between grains[57] along with chemisorption and physisorption of vapor on to the ZnO grains. Fig. 7(a) shows the layout of the inter-grain pore structure of the ZnO nanoparticles. The water vapor can easily condense due to capillary action of the pores. On exposure to moisture, there is chemisorption of water molecules on activated sites of the ZnO grains. This vapor dissociates to form hydroxyl groups when water reacts with lattice oxygen[58] generating oxygen vacancies (O_v) as per eqn (7).

$$H_2O + ZnO \leftrightarrow 2OH - Zn + O_v + 2e^- \quad (7)$$

There is an electronic interchange produced by the condensation of water vapor on the ZnO interface.[24] More water vapor layers are physisorbed on the hydroxyl layer by hydrogen bonding (Fig. 6(b)). The singly bonded water molecules are able to form continuous dipoles leading to an increase in the dielectric constant.[57] Hence, the enhancement in the capacitive signal is prominent for higher moisture content samples. In addition, the dielectric constant of ZnO itself plays an important role in enhancing the capability of the sensor. Nanocrystalline materials are well known to have a majority of atoms in grain boundaries and a very high density of surface defects.[59] Hence, the grain boundaries of ZnO nanoparticles should be rich in oxygen vacancies. These vacancies act as dipoles (Fig. 7(b)) leading to higher values of the dielectric constant.[46]

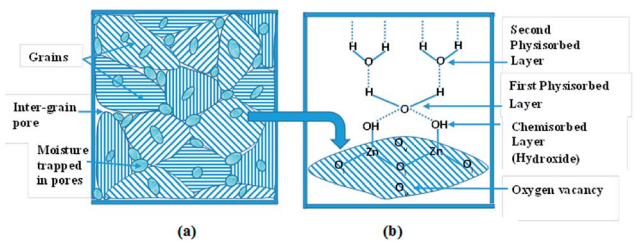

Fig. 7 (a) The inter-grain pore structure of the ZnO nanoparticles containing water vapor and (b) chemical and physical adsorption of water molecule layers on a grain along with oxygen vacancies.

4 Conclusions

ZnO nanoparticles were successfully synthesized using a wet chemical method. The XRD results reveal the formation of a hexagonal phase that have a predominant (002) plane of ZnO nanoparticles with an average crystallite size of ~16 nm. TEM results also suggest the crystallite size is in the range ~15–20 nm. FTIR and photoluminescence studies also confirm the formation of ZnO nanoparticles. BET analysis confirms a highly mesoporous structure of the ZnO nanoparticles. A blue shift in the optical band gap of the ZnO nanoparticles was observed as compared to their bulk counterpart. The surface RMS roughness for the ZnO nanoparticles is ~3 nm. Experimental observations reveal that, after film deposition, the cell shows high-moisture sensitivity and good stability. Furthermore, the sensitivity shows much higher values at lower frequencies. The maximum enhancement in sensitivity is 97.4% at 500 Hz. This study demonstrates that the ZnO nanoparticles can be used as the sensing material for enhancing the capability of moisture sensors for wheat and other grains. The fabricated sensor is cost effective and easy to operate. For the future, ZnO nanomaterials exhibit vast possibilities in moisture sensing applications for grains.

Conflicts of interest

There are no conflicts of interest to declare.

Acknowledgements

The authors are thankful to Kuldeep Kumar and Alka Monga, Panjab University, Chandigarh, India, Ishita Chakrabarti, DAV

Model School, Sector 15, Chandigarh, India, Jagvir Singh, Lethbridge College, Edmonton, Canada and Ritula Thakur, NITTTR, Sector 26, Chandigarh, India for their suggestions and motivation in completing this manuscript.

References

1 C.-Y. Lee and G.-B. Lee, *Sens. Lett.*, 2005, **3**, 1–14.
2 R. Srivastava, N. Nidhi and B. C. Yadav, *Adv. Sci. Lett.*, 2014, **20**, 917–922.
3 P. Bruno, G. Cicala, F. Corsi, A. Dragone and A. M. Losacco, *Sens. Actuators, B*, 2004, **100**, 126–130.
4 T. Islam, A. T. Nimal, U. Mittal and M. U. Sharma, *Sens. Actuators, B*, 2015, **221**, 357–364.
5 H. M. J. Al-Taii, Y. M. Amin and V. Periasamy, *Sci. Rep.*, 2016, **6**, 25519.
6 J. Qian, Z. Peng, Z. Shen, Z. Zhao, G. Zhang and X. Fu, *Sci. Rep.*, 2016, **6**, 25574.
7 S. K. Shukla, S. K. Shukla, P. P. Govender and E. S. Agorku, *Microchim. Acta*, 2016, **183**, 573–580.
8 G. Korotcenkov, V. Brinzari and B. K. Cho, *Microchim. Acta*, 2016, **183**, 1033–1054.
9 L. Yang, Y. Zheng, Z. Jiang and Z. Ren, Improvement of the capacitive grain moisture sensor, in *Computer and Computing Technologies in Agriculture V (CCTA 2011)*, ed. D. Li and Y. Chen, IFIP Advances in Information and Communication Technology, Springer, Berlin, 2012, vol. 370, pp. 300–307.
10 T. A. Blank, L. P. Eksperiandova and K. N. Belikov, *Sens. Actuators, B*, 2016, **228**, 416–442.
11 S. U. Susha Lekshmi, D. N. Singh and A. N. D. M. S. Baghini, *Measurement*, 2014, **54**, 92–105.
12 W. Bolton, *Engineering Science*, Newnes, Oxford, 5th edn, 2006.
13 Q. Qi, T. Zhang, Y. Zeng and H. Yang, *Sens. Actuators, B*, 2009, **137**, 21–26.
14 B. Weintraub, Z. Zhou, Y. Li and Y. Deng, *Nanoscale*, 2010, **2**, 1573–1587.
15 A. Torabi and V. N. Staroverov, *J. Phys. Chem. Lett.*, 2015, **6**, 2075–2080.
16 W. Wang, T. Ai and Q. Yu, *Sci. Rep.*, 2017, **7**, 42615.
17 J. Shi, Y. Liu, Q. Peng and Y. Li, *Nano Res.*, 2013, **6**, 441–448.
18 J. Guo, J. Zhang, M. Zhu, D. Ju, H. Xu and B. G. Cao, *Sens. Actuators, B*, 2014, **199**, 339–345.
19 D. Li, L. Zhao, R. Wu, C. Ronning and J. G. Lu, *Nano Res.*, 2011, **4**, 1110–1116.
20 J. Cho, Q. Lin, S. O. Yang, J. G. Simmons Jr, Y. Cheng, E. Lin, J. Yang, J. V. Foreman, H. O. Everitt, W. Yang, J. Kim and J. Liu, *Nano Res.*, 2012, **5**, 20–26.
21 K. Bhavsar, D. Ross, R. Prabhu and P. Pollard, *Nano Rev.*, 2015, **6**, 26711.
22 Z. Liang, Q. Zhang, L. Jiang and G. Cao, *Energy Environ. Sci.*, 2015, **8**, 3442–3476.
23 W. Xuan, M. He, N. Meng, X. He, W. Wang, J. Chen, T. Shi, T. Hasan, Z. Xu, Y. Xu and J. K. Luo, *Sci. Rep.*, 2014, **4**, 7206.
24 J. Herran, I. Fernandez, E. Ochoteco, G. Cabanero and H. Grande, *Sens. Actuators, B*, 2014, **198**, 239–242.
25 D. Fu, C. Zhu, X. Zhang, C. Li and Y. Chen, *J. Mater. Chem. A*, 2016, **4**, 1390–1398.
26 Y. Im, S. Kang, B. S. Kwak, K. S. Park, T. W. Cho, J. S. Lee and M. Kang, *Korean J. Chem. Eng.*, 2016, **33**, 1447–1455.
27 A. Anzlovar, K. Kogej, Z. C. Orel and M. Zigon, *Cryst. Growth Des.*, 2014, **14**, 4262–4269.
28 Y. Lv, W. Xiao, W. Li, J. Xue and J. Ding, *Nanotechnology*, 2013, **24**, 175702.
29 M. A. Basyooni, M. Shaban and A. M. E. Sayed, *Sci. Rep.*, 2017, **7**, 41716.
30 B. S. Bansod, R. Thakur and M. Singla, *Trans. Inst. Meas. Control*, 2012, **34**, 539–545.
31 B. S. Bansod and R. Thakur, *J. Sci. Ind. Res.*, 2011, **70**, 41–44.
32 H. Singh, B. S. Bansod, R. Thakur, T. Singh and J. Sharma, *Int. J. Pure Appl. Phys.*, 2017, **13**(1), 146–149.
33 M. F. Khan, A. H. Ansari, M. Hameedullah, E. Ahmad, F. M. Husain, Q. Zia, U. Baig, M. R. Zaheer, M. M. Alam, A. M. Khan, Z. A. AlOthman, I. Ahmad, G. M. Ashraf and G. Aliev, *Sci. Rep.*, 2016, **6**, 27689.
34 S. Zandi, P. Kameli, H. Salamati, H. Ahmadvand and M. Hakimi, *Phys. B*, 2011, **406**, 3215–3218.
35 D. L. Liu, J. J. Martin and N. N. Burnham, Optimal roughness for minimal adhesion, *Appl. Phys. Lett.*, 2007, **91**, 43107.
36 P. Schroer, P. Kriiger and J. Pollmann, *Phys. Rev. B*, 1993, **47**, 6971–6980.
37 J. P. Borah and K. C. Sarma, *Acta Phys. Pol., A*, 2008, **114**, 713–719.
38 S. T. Tan, B. J. Chen, X. W. Sun, W. J. Fan, H. S. Kwok, X. H. Zhang and S. J. Chua, *J. Appl. Phys.*, 2005, **98**, 013505.
39 S. T. Tan, B. J. Chen, X. W. Sun, X. Hu, X. H. Zhang and S. J. Chua, *J. Cryst. Growth*, 2005, **281**, 571–576.
40 Y. Tian, A. Merdasa, M. Peter, M. Abdellah, K. Zheng, C. S. Ponseca Jr, T. Pullerits, A. Yartsev, V. SundstrÃűm and I. G. Scheblykin, *Nano Lett.*, 2015, **15**, 1603–1608.
41 K. Mahmood, S. B. Park and H. J. Sung, *J. Mater. Chem. C*, 2013, **1**, 3138–3149.
42 S. Xu and Z. Wang, *Nano Res.*, 2011, **4**, 1013–1098.
43 K. N. Abbas and N. Bidin, Morphological driven photocatalytic activity of ZnO nanostructures, *Appl. Surf. Sci.*, 2017, **394**, 498–508.
44 E. Karber, T. Raadik, T. Dedova, J. Krustok, A. Mere, V. Mikli and M. Krunks, *Nanoscale Res. Lett.*, 2011, **6**, 359.
45 S. Kundu, S. Sain, B. Satpati, S. R. Bhattacharyya and S. K. Pradhan, *RSC Adv.*, 2015, **5**, 23101–23113.
46 P. Rejani, A. Radhakrishnan and B. Beena, *Int. J. Nano Dimens.*, 2014, **5**, 497–503.
47 F. Oba, M. Choi, A. Togo and I. Tanaka, *Science and Technology of Advanced Matererials*, 2011, **12**, 034302.
48 C. Drouilly, J. M. Krafft, F. Averseng, S. Casale, D. Bazer-Bachi, C. Chizallet, V. Lecocq, H. Vezin, H. Lauron-Pernot and G. Costentin, *J. Phys. Chem. C*, 2012, **116**, 21297–21307.
49 T. J. Jacobsson and T. Edvinsson, *Inorg. Chem.*, 2011, **50**, 9578–9586.
50 R. K. Nahar and V. K. Khanna, *Int. J. Electron.*, 1982, **52**, 557–567.
51 S. Sikarwar and B. C. Yadav, *Sens. Actuators, A*, 2015, **233**, 54–70.

52 N. Bhargava, R. Jain, I. Joshi and K. S. Sharma, *J. Environ. Nanotechnol.*, 2013, **2**, 1–5.
53 S. Thakur and P. Patil, *Sens. Actuators, B*, 2014, **1994**, 260–268.
54 N. Lazarus and G. K. Fedder, *J. Micromech. Microeng.*, 2011, **21**, 065028.
55 S. Kumar, *Solid State Physics: AIP Conference Proceedings*, 2014, vol. 1591, pp. 555–557.
56 J. Li, T. Fu, Y. Chen, B. Guan, M. Zhuo, T. Yang, Z. Xu, Q. Li and M. Zhang, *CrystEngComm*, 2014, **16**, 2977.
57 H. Farahani, R. Wagiran and M. N. Hamidon, *Sensors*, 2014, **14**, 7881–7939.
58 J. Fester, M. Garcia-Melchor, A. S. Walton, M. Bajdich, Z. Li, L. Lammich, A. Vojvodic and J. V. Lauritsen, *Nat. Commun.*, 2017, **8**, 14169.
59 J. Mao, Y. Chen, J. Pei, D. Wang and Y. Li, *Chem. Commun.*, 2016, **52**, 5985–5988.